

**Geometric Attraction-Driven Flow for  
Image Segmentation and Boundary  
Detection**

by

**Jooyoung Hahn and Chang-Ock Lee**

Applied Mathematics  
Research Report

07-04

September 17, 2007

DEPARTMENT OF MATHEMATICAL SCIENCES



# Geometric Attraction-Driven Flow for Image Segmentation and Boundary Detection <sup>\*</sup>

Jooyoung Hahn<sup>†</sup> and Chang-Ock Lee<sup>‡</sup>

Department of Mathematical Sciences  
KAIST, Daejeon, 305-701, Korea

## Abstract

Noble forces in image segmentation based on active contours models are proposed for capturing objects in the image. Contemplating the common functionality of forces in previous active contours models, we propose the geometric attraction-driven flow (GADF), the binary edge function, and the binary balloon forces to detect objects in difficult cases such as varying illumination and complex shapes. The orientation of GADF is orthogonally aligned with the boundary of object and has the opposite direction across the boundary. It prevents the leakage on the weak edge. To reduce the interference from other forces, we design the binary edge function using the property of orientation in GADF. We also design the binary balloon force based on the four-color theorem. Combining with initial dual level set functions, the proposed model captures holes in objects and multiple junctions from different colors. The result does not depend on positions of initial contours.

**Keywords:** GADF, binary edge function, binary balloon force, image segmentation, boundary detection, weak edge, multiple junctions, concave boundary, dual level set functions

## 1 Introduction

Image segmentation and boundary detection are important low-level topics in computer vision. The main goal is to capture the feature of interests in the image and the hundreds of good algorithms and methodologies have been developed based on mathematical theory and modeling. Our research is motivated by making the 3D VR (virtual reality) content of commercial products. It makes an e-catalog that customers can browse a product in three dimensional virtual space on internet markets. A common way of making the 3D VR content starts from taking many photographs of a product with different view angles in the photo studio. The most difficult step is to extract the product from the background. It seems to be relatively easy problem to detect such objects comparing with the problems of capturing some objects in natural images in [1, 2]. However, images taken in the photo studio have well-known difficulties in image segmentation even though they usually have the

---

<sup>\*</sup>This work was supported by KRF-2006-311-C00015.

<sup>†</sup>jyhahn76@amath.kaist.ac.kr

<sup>‡</sup>colee@kaist.edu

---

a. leakage on the weak edge changed smoothly from strong edges
b. inaccuracy of result depending on noise in an image
c. different results depending on positions of initial contours
d. slow convergence to concave boundaries
e. missing contours in the result on multiple junctions and holes in objects
f. many parameters in the evolution equation

---

Table 1.1: General problems in active contours for image segmentation

simple background color and small amount of noises such as JPEG artifacts. These mainly come from change of illumination, which happens naturally because of lighting conditions. Most of lighting conditions make shadows which cause weak edges between dark objects and the background. More serious weak boundaries are produced by a reflection on some parts of an object due to the bright lighting condition and properties of materials of the object. It changes colors of objects into almost white which is normally used as a background color. Note that other simple colors on a background except white are not usually used because of color bleeding effect. In addition, there are another difficulties; the boundary of objects can be highly non-convex, multiple junctions can be happened from different colors of objects, and the region of object in the image can be multiply connected, which means the object has holes inside; see Figure 4.4.

The models based on active contours have been used as successful methods in image segmentation and boundary detection. Since the original model was developed by [3], extensive research has been done in order to make up for drawbacks in Table 1.1. Note that these problems frequently come out from images taken in the photo studio. The geodesic active contours [4, 5] had a concrete mathematical theory with the level set formulation [6]. The gradient vector flow [7–9] was proposed for a fast convergence to non-convex boundaries. The curvature vector flow [10] and normalized gradient vector diffusion [11] were introduced to overcome the limitation of the gradient vector flow for capturing highly non-convex shapes. In [12], the regions-aided geometric snake was proposed for more robust detection of weak edges. The previous models rely on the edge map (2.2) or the edge function (2.4) which are obtained by the magnitude of the gradient of image. It mainly causes problems of leakage on the weak edge; see Figure 4.1. On the contrary, the active contours without edges proposed by [13, 14] does not use such functions. It may capture weak edges and it is also robust to obtain same result using different positions of initial contour. The geodesic active regions [15, 16] is a new framework of integrating the boundary-based segmentation [4, 5, 17] with the region-based segmentation [18, 19]. However, they are strongly affected by varying illumination in the image; see Figure 4.2. We will review more details in Section 2.

In this paper, we contemplate active contours models which have been mostly used in image segmentation and find common terms which play the same role in the view of forces to evolve contours. We classify them into three categories, controlling smoothness of contours, forcing contours to move from far distance toward boundaries of objects, and attracting contours much closer to the boundaries. The key to make a good model for segmentation is to construct well-designed forces which effectively move contours on the feature of interest and to reduce the interference of forces in order to maximize the role of each force. In order

to keep these facts and solve problems in Table 1.1, we propose noble forces: geometric attraction-driven flow (GADF), the binary edge function, and the binary balloon force. The main attribute of GADF is its natural and reliable representation of the boundary of objects even though there is the weak edge changed smoothly from strong edges in a color or gray image. The orientation of the GADF is orthogonally aligned with the boundary of object and two vectors across the boundary are in the opposite direction. It prevents the leakage on the weak edge even though the illumination is changed; see Figure 4.2. If we consider an image as a two dimensional manifold, the GADF is obtained by comparing two lengths of curves along the direction of the largest change in the manifold. In order to reduce interference from other forces, we design the binary edge function using the property of orientation in the GADF. At last, we design the binary balloon force based on the four-color theorem [20, 21]. It has two values, 1 or  $-1$ , which mean that contours are expanded or shrunk. The main goal of the binary balloon force is to move the initial contours toward boundaries of object regardless of positions of the contours. Combining with initial dual level set functions, it solves topological problems in Table 1.1 such as detection of holes or multiple junctions and dependency on positions of initial contours.

The rest of this paper is organized as follows. We explain the proposed model in Section 2. Considering the main role of each term in the model, we propose the GADF, the binary edge function, and the binary balloon force in Section 3. We also explain why they can handle the problems of image segmentation. In Section 4, examples and numerical aspects are illustrated with discussion about the strength and the weakness of the proposed model. The paper is concluded in Section 5.

## 2 Previous works and common terms in active contours

We briefly review active contours models which have been mostly used in image segmentation and boundary detection. The fundamental idea of active contours is to make proper forces of evolving curves in order to find the boundary of objects in the image. In this section, we find common terms which play similar role in forces to evolve curves. A classification of forces gives general ideas for designing a good evolution equation.

Let  $I: \Omega \subset \mathbf{R}^2 \rightarrow \mathbf{R}^+$  be a given image and  $\mathcal{C}(s): [0, 1] \rightarrow \Omega$  be a parameterized contour. The classical snake is to find a contour which minimizes the functional [3]:

$$E(\mathcal{C}) = \alpha \int_0^1 |\mathcal{C}'(s)|^2 ds + \beta \int_0^1 |\mathcal{C}''(s)|^2 ds - \gamma \int_0^1 |\nabla G_\sigma * I(\mathcal{C}(s))|^2 ds,$$

where  $\alpha$ ,  $\beta$ , and  $\gamma$  are positive constants and  $G_\sigma * I$  is the convolution of an image  $I$  with the two-dimensional Gaussian kernel with the standard deviation  $\sigma$ . The first two terms in the functional control tension and rigidity of the contour and the last term attracts the contour towards the object in the image. The minimizer  $\mathcal{C}$  is obtained at the points of maximizing  $|\nabla G_\sigma * I|^2$  with keeping smoothness of the contour. Two drawbacks have been discussed in many papers; the first is a dependence on positions of initial contours [17] and the second is a poor convergence to concave boundaries of the object [22]. One of promising solution [7, 8] was proposed by using the gradient vector flow (GVF) which is a diffused bidirectional external force. It is obtained by a steady state solution of partial differential

equations:

$$\begin{aligned}\frac{\partial}{\partial t}v(x, t) &= \mu\Delta v - (v - \nabla f) |\nabla f|^2, \\ v(x, 0) &= \nabla f(x),\end{aligned}\tag{2.1}$$

where  $\mu$  is a constant and  $f$  is an edge map which has higher values at edges, for example,

$$f = |\nabla G_\sigma * I|^2.\tag{2.2}$$

In the diffusion process (2.1), the second term makes a smooth change of the vectors from edges to homogeneous regions and the third term keeps the vectors near edges pointing to the boundary of objects. Even though it was a successful approach to overcome problems in the classical snakes, there are still same drawbacks about positioning of initial contours [12, 23] and capturing concave boundaries [10, 11].

An equivalence relation between parametric active contours [3, 7] and geometric active contours [4] was established [9] by using the level set method [6]. Let  $\phi$  be a Lipschitz function such that

$$\Gamma_\phi: \mathcal{C} = \{x \in \Omega \mid \phi(x, 0) = 0\}$$

and evolving curves at time  $t$  be the zero level set of  $\phi(x, t)$ . The curve evolution in the GVF from the general formulation [9] is

$$\frac{\partial}{\partial t}\phi = \left(\alpha\kappa + \beta\kappa^3 - \nabla \left(\nabla(\beta\kappa) \cdot \nabla\phi^\perp\right) \cdot \nabla\phi^\perp\right) |\nabla\phi| - F_G \cdot \nabla\phi,\tag{2.3}$$

where  $\kappa$  is the curvature of level curves of  $\phi$ ,  $\nabla\phi^\perp$  is the orthonormal direction to  $\nabla\phi$ , and  $F_G$  is the GVF, *i.e.*, the steady state solution of (2.1).

A geodesic model is to find a contour which minimizes the functional [5]:

$$E(\mathcal{C}) = \int_0^1 |\mathcal{C}'(s)| g(|\nabla I(\mathcal{C}(s))|) ds,$$

where an edge function  $g$  is defined on  $[0, \infty)$ , decreasing,  $g(0) = 1$ , and  $g(r) \rightarrow 0$  as  $r \rightarrow \infty$ , for example,

$$g = \frac{1}{1 + |\nabla G_\sigma * I|^2}.\tag{2.4}$$

The minimizer  $\mathcal{C}$  is the contour of the minimum length in the modified Euclidean metric  $g(|\nabla I(\mathcal{C}(s))|) ds$ . It is obtained on points of minimizing the edge function  $g$ . The geodesic approach allows to connect classical snakes and geometric active contours (GAC) [4]. From this connection, the general geodesic active contours model has a level set formulation

$$\frac{\partial}{\partial t}\phi = g\kappa |\nabla\phi| + g\eta |\nabla\phi| + \nabla g \cdot \nabla\phi,\tag{2.5}$$

where  $\kappa$  is the curvature of level curves of  $\phi$  and  $\eta$  is a constant. Although the existence, uniqueness, stability, and consistency of the formulation were proved from the notion of viscosity solutions [24], same problems of the GVF are discussed in [12, 14, 15, 23]

Active contours without edges (ACWE) [14] is a significant breakthrough in active contours because the model does not depend on the edge function  $g$ . It is to find a contour  $\mathcal{C}$  and two constants  $\mu_1$  and  $\mu_2$  which minimize the functional:

$$E(\mu_1, \mu_2, \mathcal{C}) = \alpha \int_{\Omega} |\nabla H(\phi(x))| dx + \eta \int_{\Omega} H(\phi(x)) dx \\ + \lambda_1 \int_{\Omega} |I(x) - \mu_1|^2 H(\phi(x)) dx + \lambda_2 \int_{\Omega} |I(x) - \mu_2|^2 (1 - H(\phi(x))) dx,$$

where  $H$  is the one-dimensional Heaviside function and  $\phi$  is the level set function whose zero level set is the contour  $\mathcal{C}$ . If  $\eta = 0$ , the minimizer  $\mu_1$ ,  $\mu_2$ , and  $\mathcal{C}$  is same as the minimizer of the Mumford-Shah functional [25] with the restriction to bimodal functions which have two values in the image, *i.e.*,  $\mu_1$  on outside  $\mathcal{C}$  and  $\mu_2$  on inside  $\mathcal{C}$ . The level set formulation is

$$\frac{\partial}{\partial t} \phi = \alpha \kappa |\nabla \phi| + \left( \lambda_2 (I - \mu_2)^2 - \lambda_1 (I - \mu_1)^2 - \eta \right) |\nabla \phi|, \quad (2.6)$$

where  $\mu_1$  and  $\mu_2$  are average of image on outside of  $\mathcal{C}$  and inside of  $\mathcal{C}$  respectively and  $\kappa$  is the curvature of level curves of  $\phi$ . The limitation of bimodal segmentation is overcome by using multiphase level set framework [13] and image statistics over known number of region types [26]. Even though just one level set function is used, all of the phase in the image can be segmented by a special set of basis functions in [27]. The existence of global minimum invariant to the initialization of level set function and fast convergence are recently proposed in [28] by using a modified fitting term.

Geodesic active regions (GAR) [15, 16] is a new framework of integrating the boundary-based segmentation [4, 5, 17] with the region-based segmentation [18, 19]. There have been other efforts to combine boundary information with region information for frame partition problems [19, 29]. The segmentation of vector valued images based on geodesic active regions was introduced by [30] and the level set formulation for gray image is

$$\frac{\partial}{\partial t} \phi = \alpha \kappa |\nabla \phi| + \left( \log \frac{\sigma_2^2}{\sigma_1^2} - \frac{(I - \mu_1)^2}{\sigma_1^2} + \frac{(I - \mu_2)^2}{\sigma_2^2} \right) |\nabla \phi|, \quad (2.7)$$

where  $\kappa$  is the curvature of level curves of  $\phi$ . The values  $\mu_1$  and  $\sigma_1$  are the average and the standard deviation of the image on  $\phi > 0$ , respectively. The values  $\mu_2$  and  $\sigma_2$  are the average and the standard deviation of the image on  $\phi < 0$ , respectively. Note that it is easily generalized to color images with multi-dimensional Gaussian distributions and multiple regions with an additional coupling terms [31] and multiple level set functions.

Carefully examining the functionality of each term in (2.3), (2.5), (2.6), and (2.7), it is noted that they have common terms which have the same role in view of forces to evolve contours. We classify them into three categories, controlling smoothness of contours  $F_s$ , forcing contours to move from far distance toward the boundaries of objects  $F_b$ , and attracting contours much closer to the boundaries  $F_a$ . Table 2.1 compares four models of active contours in the level set formulation:

$$\frac{\partial}{\partial t} \phi = F_s |\nabla \phi| + F_b |\nabla \phi| + F_a \cdot \nabla \phi. \quad (2.8)$$

	GVF	GAC	ACWE	GAR <sup>a</sup>
$F_s$	$-\nabla (\nabla (\beta\kappa) \cdot \nabla \phi^\perp) \cdot \nabla \phi^\perp$	$g\kappa$	$\alpha\kappa$	$\alpha\kappa$
$F_b$	0	$g\eta$	$\lambda_2 (I - \mu_2)^2$	$\log \sigma_2^2 - \log \sigma_1^2$
$F_a$	$-F_G$	$\nabla g$	$-\lambda_1 (I - \mu_1)^2 - \eta$	$+\frac{(I - \mu_2)^2}{\sigma_2^2} - \frac{(I - \mu_1)^2}{\sigma_1^2}$

Table 2.1: Comparison of active contours based on (2.8).  $F_s$  is to control smoothness of contours,  $F_b$  is to force contours to move from far distance toward the boundary of objects,  $F_a$  is to attract contours much closer to the boundary.

<sup>a</sup> It is a simplified form [30] of the original GAR [16].

Note that  $F_b$  is also called the spatially varying balloon force [17], the combination of  $F_b$  and  $F_a$  is considered as region force [30], and the original model of GAR [16] can has each term in the above equation.

The key to make a good evolution equation for segmentation is to construct well-designed forces which effectively move contours on the feature of interest and to reduce interference of forces in order to maximize the role of each force. In order to keep these facts and solve problems in Table 1.1, we propose noble forces, the GADF  $F_a$ , the binary balloon force  $F_b$ , and the binary edge function  $g_b$  in the level set formulation:

$$\begin{aligned} \frac{\partial}{\partial t} \phi(x, t) &= \alpha\kappa |\nabla \phi| + g_b F_b |\nabla \phi| + (1 - g_b) F_a \cdot \nabla \phi, \\ \phi(x, 0) &= \phi_0(x), \end{aligned} \quad (2.9)$$

where  $\alpha$  is a constant,  $\kappa$  is the curvature of level curves of  $\phi$ , and  $\phi_0(x)$  is the initial level set function. The first term  $\alpha$  controls smoothness of contours. The second term  $F_b$  is the binary balloon force in Section 3.3 which moves contours from far distance toward boundaries. Combining with initial dual level set functions and the four-color theorem [20, 21], it solves topological problems in Table 1.1 such as detection of holes or multiple junctions and dependency on positions of initial contours. The third force  $F_a$  is the GADF in Section 3.1 which accurately attracts contours much closer to boundaries of objects even though there is the weak edge changed smoothly from strong edges. The binary edge function  $g_b$  in Section 3.2 minimizes interference between the GADF and the binary balloon force in order to maximize the role of each force.

### 3 Segmentation using GADF

#### 3.1 Geometric attraction-driven flow

##### 3.1.1 Formulation

For a scalar image  $I$ , the geometric attraction-driven flow (GADF) has the direction of pointing local maxima of the strength of edges  $|\nabla I|$  along the gradient direction  $\nabla I$ . To find such a direction for each point  $x$  in a color image, we need to estimate the strength of edges and a gradient direction by using values of  $I$  on a neighborhood of  $x$  and an algorithm to choose one of two directions  $\pm\nabla I$  which points local maxima of the approximated strength of edges. The main attribute of GADF is its natural and reliable representation of the boundary of objects even though there is the weak edge changed smoothly from strong edges in a color or gray image. Note that such a weak edge looks in a shape of ridge in the strength of edges.

Let us first explain the basic idea of GADF. We consider a scalar image  $I: \Omega \subset \mathbf{R}^2 \rightarrow \mathbf{R}^+$ , which is smooth enough. Since we may assume that the intensity near boundaries of an object changes rapidly from one homogeneous region to another homogeneous region, we define a point  $x$  in  $\Omega$  as an edge point if the second directional derivative of  $I$  at  $x$  along  $\nabla I(x)$  vanishes:

$$x: \text{edge point} \iff u_x''(s)|_{s=0} = 0, \quad u_x(s) = I\left(x + s \frac{\nabla I(x)}{|\nabla I(x)|}\right). \quad (3.1)$$

For a smooth scalar function  $y$  on the real line, the following is easily proved: If  $y' \neq 0$  and  $y'' \neq 0$  in  $(x - r, x + r)$  for some  $r > 0$ , for any positive  $\epsilon \leq r$ , we have

$$\text{sgn}\left(\int_x^{x+\epsilon} y'(s) ds - \int_{x-\epsilon}^x y'(s) ds\right) = \text{sgn}(y''(x)),$$

where

$$\text{sgn}(x) \equiv \begin{cases} x/|x| & \text{if } x \neq 0, \\ 0 & \text{if } x = 0. \end{cases}$$

Motivated by this statement, we define a vector field  $F_a(x)$  by

$$F_a(x) = \text{sgn}(\ell(x)) \frac{\nabla I(x)}{|\nabla I(x)|}, \quad \forall x \in \Omega, \quad (3.2)$$

where

$$\begin{aligned} \ell(x) &= \int_0^\epsilon u_x'(s) ds - \int_{-\epsilon}^0 u_x'(s) ds \quad \text{for a small } \epsilon > 0, \\ u_x(s) &= I\left(x + s \frac{\nabla I(x)}{|\nabla I(x)|}\right). \end{aligned} \quad (3.3)$$

Then the orientation of  $F_a$  at each point  $x \in \Omega$  is one of two directions  $\pm\nabla I(x)$  and it points to the edge point along the straight line  $x + s \frac{\nabla I(x)}{|\nabla I(x)|}$ , which is the local maxima of strength of edges  $|\nabla I|$  along the straight line.



The vector field  $F_a$  in (3.2) can be naturally extended to a color image  $I: \Omega \subset \mathbf{R}^2 \rightarrow (\mathbf{R}^+)^3$  after the strength of edges and the gradient direction are properly estimated in the color image. Recently, [32] proposed the nonlinear structure tensor which contains local features of the image [33]. We use the same nonlinear diffusion

$$\begin{aligned} \frac{\partial \mathbf{M}(x, t)}{\partial t} &= \nabla \cdot \left( h \left( \sum_{i,j=1}^2 |\nabla M_{ij}(x, t)|^2 \right) \nabla \mathbf{M}(x, t) \right), \\ \mathbf{M}(x, 0) &= \sum_{k=1}^3 \nabla I_k(x) \nabla I_k(x)^T, \end{aligned} \quad (3.4)$$

where  $T$  denotes the transpose and  $h(x) = 1/\sqrt{1+x}$ . Denote  $v_\Lambda(x)$  and  $v_\lambda(x)$  as normalized eigenvectors corresponding to the maximum eigenvalue  $\Lambda(x)$  and the minimum eigenvalue  $\lambda(x)$ , respectively, in a diffused tensor  $\mathbf{M}$ . We consider  $v_\Lambda(x)$  as the estimated gradient direction in a color image. Note that  $v_\Lambda(x)$  is computed in a gray image by changing the initial condition of the nonlinear diffusion equations.

Now, we define GADF  $F_a(x)$  with the estimated gradient direction  $v_\Lambda(x)$  in a color image:

$$F_a(x) = \text{sgn}(\ell(x)) v_\Lambda(x), \quad (3.5)$$

where

$$\begin{aligned} \ell(x) &= \int_0^\epsilon |u'_x(s)| ds - \int_{-\epsilon}^0 |u'_x(s)| ds \quad \text{for a small } \epsilon > 0, \\ u_x(s) &= I(x + sv_\Lambda(x)). \end{aligned} \quad (3.6)$$

Note that the above integrals measure the lengths of the curve  $u_x(s)$  in  $\mathbf{R}^3$ . If we regard  $I$  in a small neighborhood of  $x$  as a local coordinate patch for representing two dimensional manifold  $\mathcal{M}$ , the integrand is written by using the first fundamental form  $\mathcal{I}_p(v)$ ,  $p \in \mathcal{M}$  and  $v \in T_p\mathcal{M}$ , where  $T_p\mathcal{M}$  is the tangent space of  $\mathcal{M}$  at  $p$ :

$$\begin{aligned} |u'_x(s)|^2 &= \mathcal{I}_{u_x(s)}(u'_x(s)) \\ &= v_\Lambda(x)^T \left( \sum_{k=1}^3 \nabla I_k(c_x(s)) \nabla I_k(c_x(s))^T \right) v_\Lambda(x), \end{aligned}$$

where  $c_x(s) = x + sv_\Lambda(x)$ . Since the nonlinear structure tensor  $\mathbf{M}$  is a diffused tensor from the metric tensor  $\sum_{k=1}^3 \nabla I_k \nabla I_k^T$ , we replace the first fundamental form with

$$\mathbf{M} = \Lambda v_\Lambda v_\Lambda^T + \lambda v_\lambda v_\lambda^T.$$

Then, we obtain the integrand in (3.6) as

$$|u'_x(s)|^2 = \Lambda(c_x(s)) (v_\Lambda(c_x(s)) \cdot v_\Lambda(x))^2 + \lambda(c_x(s)) (v_\lambda(c_x(s)) \cdot v_\lambda(x))^2. \quad (3.7)$$

As mentioned in [32], the vector  $v_\Lambda$  in the nonlinear structure tensor is robust to noises and has filling-in effect of orientation information from the boundary of objects to homogenous

regions. The GADF also has same properties because it takes either  $v_\Lambda$  or  $-v_\Lambda$ . The propagation of the orientation information from edges is crucial to construct the binary edge function in Section 3.2.

Note that (3.5) is equal to (3.2) in a scalar image. To see this, assume that  $x \in \Omega$  is near the boundary of objects in a gray image. If two integrals in (3.6) are approximated by the trapezoidal rule with  $\epsilon = 1$ , then, from the computation of  $|u'_x(s)|$  in (3.7), we have

$$\begin{aligned}\ell(x) &= \int_0^1 |u'_x(s)| ds - \int_{-1}^0 |u'_x(s)| ds \\ &\simeq \frac{1}{2} (|u'_x(1)| - |u'_x(-1)|) \\ &= \frac{1}{2} \left[ \Lambda(x_f) (v_\Lambda(x_f) \cdot v_\Lambda(x))^2 + \lambda(x_f) (v_\lambda(x_f) \cdot v_\Lambda(x))^2 \right]^{\frac{1}{2}} \\ &\quad - \frac{1}{2} \left[ \Lambda(x_b) (v_\Lambda(x_b) \cdot v_\Lambda(x))^2 + \lambda(x_b) (v_\lambda(x_b) \cdot v_\Lambda(x))^2 \right]^{\frac{1}{2}}\end{aligned}$$

where  $x_f = x + v_\Lambda(x)$  and  $x_b = x - v_\Lambda(x)$ . Since  $x$  is near the boundaries, we may assume that

$$v_\Lambda(x_b) \parallel v_\Lambda(x) \quad \text{and} \quad v_\Lambda(x) \parallel v_\Lambda(x_f),$$

where the notation  $v_1 \parallel v_2$  means that two vectors are parallel. If the gray image is smooth enough,  $\Lambda$  and  $v_\Lambda$  can be replaced by the initial condition in (3.4), *i.e.*,  $\Lambda(x) = |\nabla I(x)|^2$  and  $v_\Lambda(x) = \frac{\nabla I(x)}{|\nabla I(x)|}$ , and we obtain

$$\ell(x) = \frac{\Lambda(x_f)^{\frac{1}{2}} - \Lambda(x_b)^{\frac{1}{2}}}{2} = \frac{|\nabla I(x_f)| - |\nabla I(x_b)|}{2}.$$

The sign of  $\ell(x)$  is simply the sign of finite difference approximation of the first order directional derivative of  $|\nabla I|$  at  $x$  along the straight line  $x + s \frac{\nabla I(x)}{|\nabla I(x)|}$ . Since

$$u''_x(s) \Big|_{s=0} = f'_x(s) \Big|_{s=0},$$

where

$$u_x(s) = I \left( x + s \frac{\nabla I(x)}{|\nabla I(x)|} \right) \quad \text{and} \quad f_x(s) = \left| \nabla I \left( x + s \frac{\nabla I(x)}{|\nabla I(x)|} \right) \right|,$$

and due to the smoothness of gray image, the GADF in (3.5) and the vector field in (3.2) are exactly same for a smooth gray image. That is, the GADF is a natural extension of (3.2) to a color image. Note that the GADF is also computed in a gray image by changing the initial condition of the nonlinear diffusion equations (3.4).

### 3.1.2 Comparison with other attraction terms

The attraction terms which have been mostly used in active contours are the GVF in (2.3) [7–9] and the gradient of edge function in (2.5) [4, 5]. The right orientation of the vector in the attraction term should be orthogonally aligned with the boundary of object and

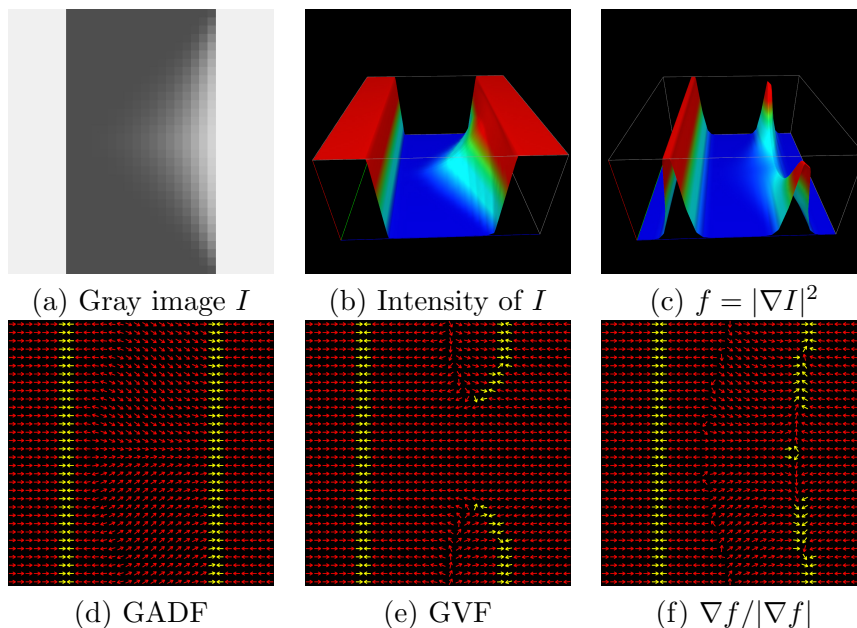


Figure 3.1: We compare the orientation of GADF with the orientation of the GVF and the gradient of edge function  $\nabla g$ . Note that  $\nabla g \parallel \nabla f$  where  $f$  is the edge map. If two vectors have opposite direction, they are highlighted with the yellow color in (d), (e), and (f). Clearly, the GADF in (a) has better information than the GVF and the gradient of edge function along the boundary of object.

two vectors across the boundary should have the opposite direction. The former property is to attract effectively the contour close to the boundary and the latter one is to force the contour to stop exactly on the boundary. In the view of these properties, we compare the orientation of the GADF in (3.5) with the orientation of vectors in the two other attraction terms.

To make it simple, we consider just a smooth scalar image  $I: \Omega \rightarrow \mathbf{R}^+$ . Note that the GVF keeps the orientation of  $\nabla f$  on the strong edges, but it is homogeneously diffused from  $\nabla f$  on weak edges. Therefore, we compare the orientation of the GADF with the orientation of  $\nabla f$  and  $\nabla g$ . For the edge function  $f$  in (2.2) and the edge map  $g$  in (2.4), we easily obtain that

$$\nabla f(x) \parallel \nabla g(x) \quad \text{and} \quad \nabla f(x) \parallel \mathcal{H}_x(I)\nabla I,$$

where  $\mathcal{H}_x(I)$  is the Hessian matrix of  $I$  at  $x$ . It is clear that the orientation of the GADF and  $\nabla f$  is same on the strong edges because the image  $I$  is not changed along the isophotes; see the left side of the object in Figure 3.1. However, it is quite different orientation between the GADF and  $\nabla f$  on the weak edge changed smoothly from strong edges; see the right side of the object in Figure 3.1. The difference is obvious because  $\nabla f$  is transformed by the Hessian matrix from  $\nabla I$ , but the GADF takes one of two directions,  $\nabla I$  or  $-\nabla I$ . It is observed that the GADF has better orientation than the other two vectors near the weak edge changed smoothly from strong edges.

### 3.2 Binary edge function

We propose the binary edge function to reduce the interference between the GADF and the binary balloon force in (2.9). Even though we have well-designed forces which effectively move contours on the feature of interest, if a force interferes with other forces, we will lose good properties of each force for segmentation. Hence, in order to maximize the performance of the well-designed forces, when one force is acting on contours, it is crucial to reduce interference between forces. We use the property of orientation of GADF to construct the binary edge function.

To attain the goal, we divide the domain  $\Omega$  of the image  $I$  into two disjoint parts  $\Omega_a$  and  $\Omega_b$  such that

$$\Omega_a = \delta_S(\Omega_E), \quad \Omega_b = \Omega \setminus \Omega_a, \quad (3.8)$$

where

$$\Omega_E = \{x \in \Omega \mid F_a(x^*) \cdot F_a(x) < 0 \text{ and } x^* = x + F_a(x)\}$$

and  $\delta_S(X)$  is the dilation of a set  $X$  by a structuring element  $S$  of the  $3 \times 3$  window centered at  $x \in X$ . The dilation is needed to make compatibility with the fast local level set method [34] to solve the proposed model (2.9). Since the GADF is a vector flow which locally points to the edge point (3.1) from each side of edges, the set  $\Omega_a$  is the collection of points in  $\Omega$  which are near the edge points. Therefore, the property of attraction in the GADF should be activated on  $\Omega_a$  and the binary balloon force controls the evolving contours on the other region  $\Omega_b$ . It makes a natural definition of the binary edge function:

$$g_b(x) = \begin{cases} 0 & \text{if } x \in \Omega_a, \\ 1 & \text{if } x \in \Omega_b. \end{cases} \quad (3.9)$$

In other words, the binary edge function  $g_b$  makes the GADF to be applied on the region  $\Omega_a$  which are near the boundary of objects and the binary balloon force to be applied on the other region  $\Omega_b$  which are distant from the boundaries. The only remaining explanation in the proposed model is how to design the binary balloon force which plays a role to move contours into  $\Omega_a$ .

### 3.3 Binary balloon force

In this section, we explain how to construct the binary balloon force which moves contours into  $\Omega_a$  the complement of the support of the binary edge function. Since the balloon force makes contours expand or shrink, we define the binary balloon force as a function on  $\Omega_b$  whose values are just of two kinds, 1 or  $-1$ . Combining with initial dual level set functions, the position of initial contours is as arbitrary as the models of ACWE [13,14] and GAR [16,30]. Applying the four-color theorem [21] to construct the binary balloon force, it is capable of capturing holes and multiple junctions in an image. Note that the problem of slow convergence to concave boundaries is easily solved because we apply the constant force to contours in the region  $\Omega_b$  which is not close to the boundaries.

To understand the full construction of the binary balloon force, we start with the simplest case in Figure 3.2-(a); the object in the image does not have holes and multiple junctions.

$F_b$ $\Gamma_{\pm\phi_0}$		Case I		Case II		Case III		Case IV	
		$\Omega_1$	$\Omega_2$	$\Omega_1$	$\Omega_2$	$\Omega_1$	$\Omega_2$	$\Omega_1$	$\Omega_2$
		1	1	-1	-1	1	-1	-1	1
$\phi_0$	Inside	✓	–	✓	–	✓	–	–	✓
	Outside	✓	–	–	–	–	–	–	✓
	Enclosed	–	✓	✓	–	✓	–	–	–
	Across	–	–	–	–	✓	–	–	✓
$-\phi_0$	Inside	–	✓	–	✓	–	✓	–	✓
	Outside	–	✓	✓	–	✓	–	–	–
	Enclosed	✓	–	–	–	–	–	–	✓
	Across	–	–	–	–	✓	–	–	✓

Table 3.1: When the proposed active contours model (2.9) is used, we check the success of capturing the object for different  $F_b$  and different positions of zero level set  $\Gamma_{\phi_0}$  of the level set function  $\phi_0$ . Note that, even though  $\Gamma_{\phi_0} = \Gamma_{-\phi_0}$ , they give different results. Four different positions of the initial contour  $\Gamma_{\phi_0}$  and the regions  $\Omega_1$  and  $\Omega_2$  are shown in Figure 3.2. Notice that the results of using  $F_b$  with  $\phi_0$  and  $-F_b$  with  $-\phi_0$  in the Cases III and IV are exactly same. We call the pair of level set functions  $\phi_0$  and  $-\phi_0$  as initial dual level set functions.

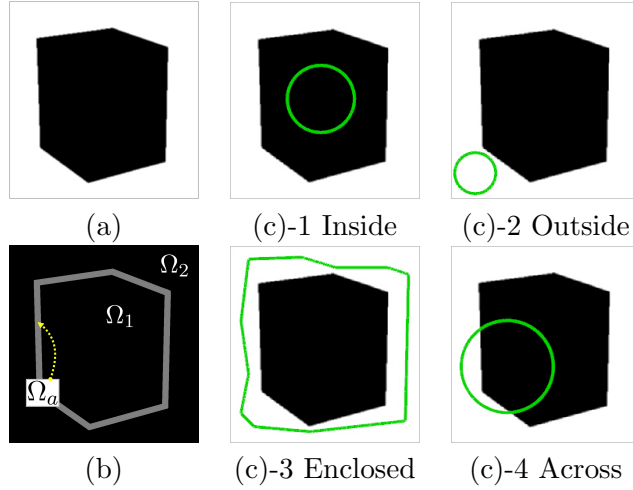


Figure 3.2: (a) is the original image and the black object is placed in the middle. (b) shows the regions in (3.8) after the binary edge function is obtained. We denote  $\Omega_1$  and  $\Omega_2$  as connected components of  $\Omega_b$  which is the support of the binary edge function. (c) is different initial contours  $\Gamma_{\phi_0}$ . Note that the initial level set function  $\phi_0$  is positive inside the contour and negative outside the contour.

First of all, we focus on making the proposed model capture the object regardless of the position of initial contours after we properly assign two values 1 or  $-1$  to the binary balloon force. Dividing the region into two connected components  $\Omega_1$  and  $\Omega_2$  in Figure 3.2-(b), we investigate all of possible cases to assign values on each region and place different initial contours; see Table 3.1. When the initial contour is placed across the object, the Cases I and II fail to capture the object. The other cases also have some initial positions which cannot capture the object. However, solving the proposed model twice for the Cases III and IV, the object is captured all the time independent of the position of the initial curve. In fact, instead of using different cases of  $F_b$ , we use the dual initial level set functions

$$\phi(x, 0) = \phi_0(x) \text{ and } -\phi_0(x) \quad (3.10)$$

because the results of using  $F_b$  with  $\phi_0$  and  $-F_b$  with  $-\phi_0$  in the Cases III and IV are exactly same. Note that, in the view of evolving contours, these functions make bidirectionally evolving contours from the initial contour. The Figure 3.3 shows that the proposed model has the capability of capturing the object regardless of the position of initial contours. The initial condition is as arbitrary as the models of ACWE [13, 14] and GAR [16, 30].

Now, we are ready to deal with more complicated case in Figure 3.4-(a); the object in the image has holes and multiple junctions. The key feature of the binary balloon force  $F_b$  in Figure 3.3 is that it has two different values 1 or  $-1$  across the adjacent connected components in  $\Omega_b$  in order to capture the object regardless of the position of initial contours. The domain of image is decomposed into  $\Omega_a$  and  $\Omega_b$  and the region  $\Omega_b$  is divided into several connected components  $\Omega_i$ 's. To obtain the general boundary detection algorithm, we use the four-color theorem [21]. Then each component  $\Omega_i$  is labeled with red, green, blue, and yellow such that no two colors across adjacent components are same. Note that there is a good algorithm [20] to assign such colors. Based on four colors, we solve the proposed model (2.9) twice with two different profiles of the binary balloon force,  $F_b^1$  and  $F_b^2$ :

$$F_b^1(x) = \begin{cases} -1 & \text{if } x \in \Omega_i \text{'s labeled with red or yellow,} \\ 1 & \text{if } x \in \Omega_i \text{'s labeled with green or blue,} \\ 0 & \text{if } x \in \Omega_a, \end{cases} \quad (3.11)$$

$$F_b^2(x) = \begin{cases} -1 & \text{if } x \in \Omega_i \text{'s labeled with green or yellow,} \\ 1 & \text{if } x \in \Omega_i \text{'s labeled with red or blue,} \\ 0 & \text{if } x \in \Omega_a. \end{cases} \quad (3.12)$$

Recalling the two component case in Figure 3.3,  $F_b^1$  with the dual level set functions capture boundaries between regions with red or yellow and regions with green or blue. Similarly  $F_b^2$  captures boundaries between regions with green or yellow and regions with red or blue. Combination of these results detects all boundaries between four colors; see Figure 3.4.

## 4 Examples and numerical aspects

We briefly explain the procedure to solve the proposed model (2.9) with some numerical aspects. We use the AOS scheme [35] to solve the nonlinear diffusion (3.4) with the specified final time  $T_0$ . The explicit Euler scheme is used for time discretization of (2.9). The simple

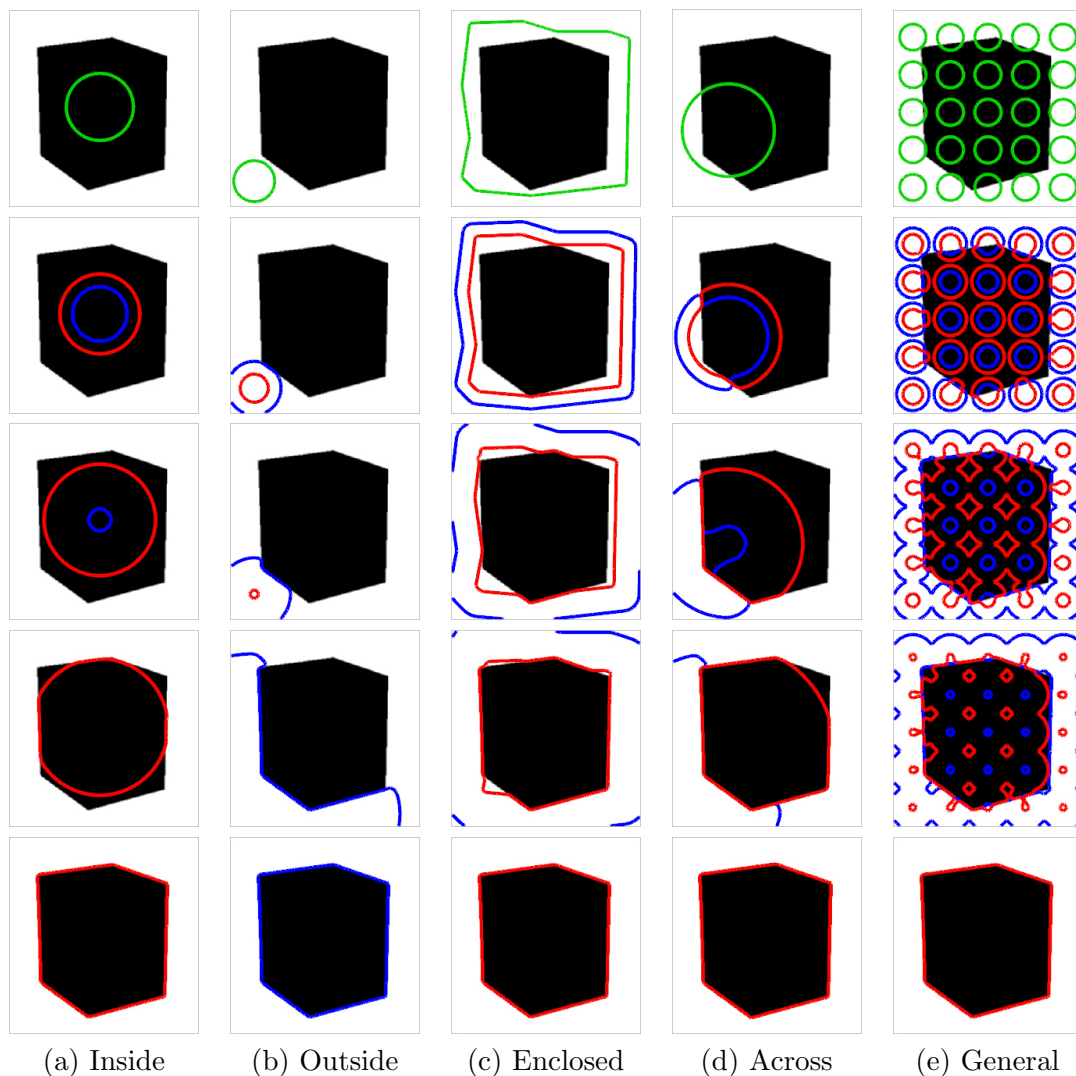


Figure 3.3: From top to bottom, the evolving contours of the proposed model (2.9) are shown with different positions of the initial contour. We use dual level set functions,  $\phi_0$  and  $-\phi_0$ , as the initial condition and the binary balloon force as the Case III in Table 3.1. The level set function  $\phi_0$  is positive inside the contour and negative outside the contour. The red and blue contour are evolved from  $\phi_0$  and  $-\phi_0$ , respectively. Notice that, by using initial dual level set functions and the proper binary balloon force, the proposed model has the capability of capturing the object regardless of the position of initial contours.

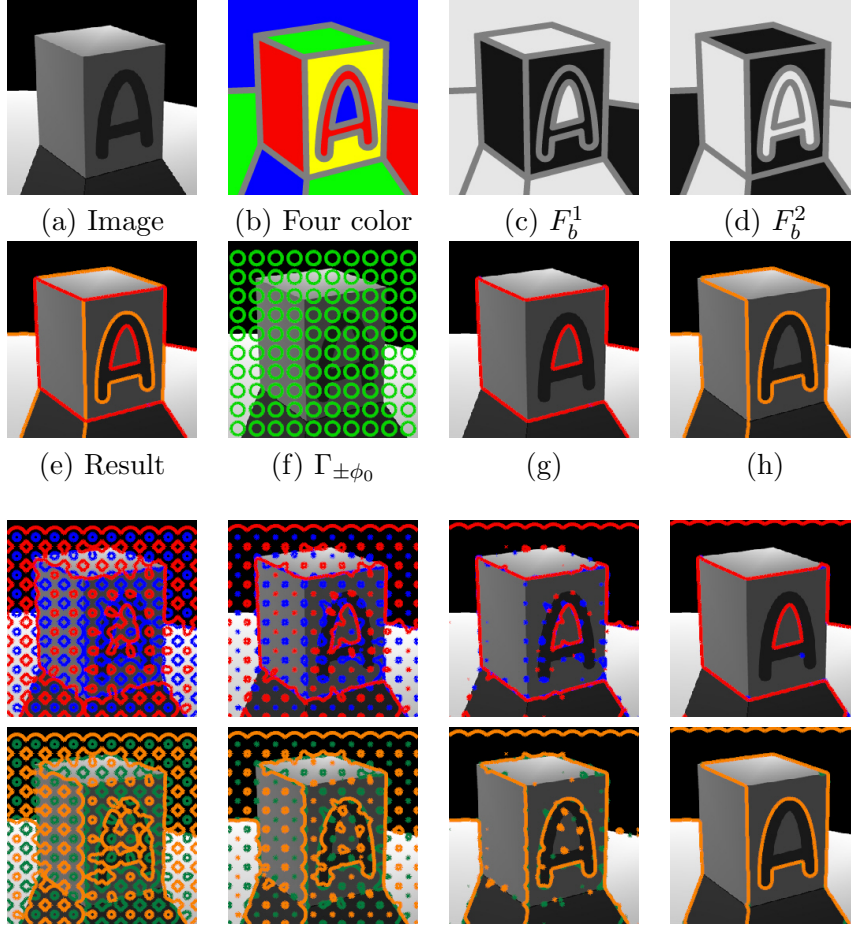


Figure 3.4: (a) is the original image and the object in the middle has holes and multiple junctions. The gray region in (b) is  $\Omega_a$  and four colors are labeled on connected components of  $\Omega_b$  in (3.8) based on the four-color theorem. (c) and (d) are the profiles of  $F_b^1$  and  $F_b^2$ ; white, gray, and black represent 1, 0, and  $-1$ , respectively. The green contours in (f) are initial contours. The contours in (g) are the result of the proposed model (2.9) from initial dual level set functions with the binary balloon force  $F_b^1$ . The contours in (h) are obtained in the same way from  $F_b^2$ . Combining two contours in (g) and (h), the final result in (e) is obtained. The evolving contours from (f) to (g) and (h) are shown in the third and the fourth row, respectively



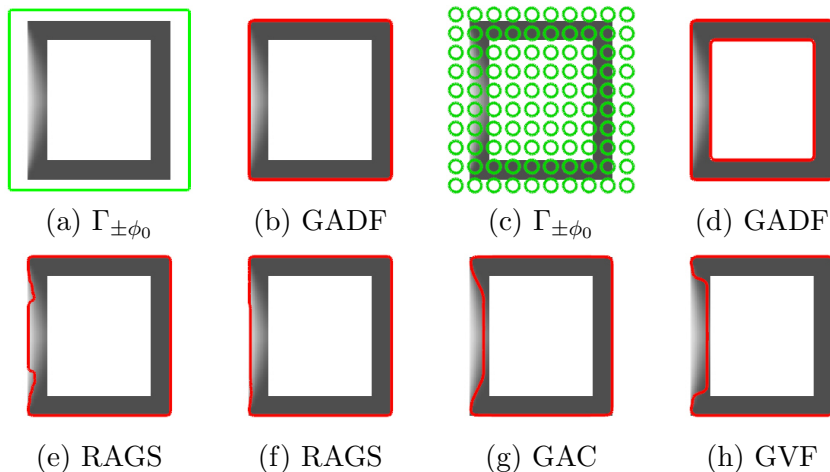


Figure 4.1: The contours in (b) and (d) are the results of the proposed model (2.9) from the initial contours in (a) and (c), respectively. The GADF captures the weak edge which is the left part of the rectangle frame. The RAGS in (f) also capture the weak edge when the region map gives the correct information. In (e) and (f), we use two different region maps to obtain the result of the RAGS. The contour from the GAC and the GVF passes by the weak edge. Note that we capture the whole frame in (d) by using the general type of initial contours in (c).

upwind scheme and the nonoscillatory upwind scheme are used for space discretization; see [36] for details of numerical schemes. For a computational efficiency, the fast local level set method [34] is applied. A stopping criterion is given by measuring an error in a small band [31]:

$$E_{\phi^{n+1}} \equiv \frac{1}{|\Omega_{\zeta}^{\phi^n}|} \int_{\Omega_{\zeta}^{\phi^n}} |\phi^{n+1}(x) - \phi^n(x)| dx, \quad (4.1)$$

$$\Omega_{\zeta}^{\phi^n} \equiv \left\{ x \in \Omega \mid |\phi^n(x)| \leq \zeta \right\},$$

where  $\zeta = 1.5$  and  $n$  is an index for time discretization. We practically stop numerical iteration with the criterion  $E_{\phi^n} < 10^{-5}$ .

From synthetic and real images, we discuss about the strength and the weakness of the proposed model and compare with some results from other methods. The first example in Figure 4.1 shows the prevention of the leakage on the weak edge changed smoothly from strong edges. The proposed model captures the boundary of object without the leakage and contours from the GAC and the GVF pass by the weak edge because the GADF basically takes the orientation of the gradient of image, while the orientation of the attraction term in the GAC and the GVF are affected by the Hessian matrix of the image. The results of RAGS depend on region maps obtained from [37] with different parameters. It works when the region map is properly obtained.

The image in Figure 4.2 has varying illumination and highly concave shape. Even though the illumination is changed on the background, the orientation of GADF is orthogonally aligned with the boundary of object and two vectors across the boundary have the opposite

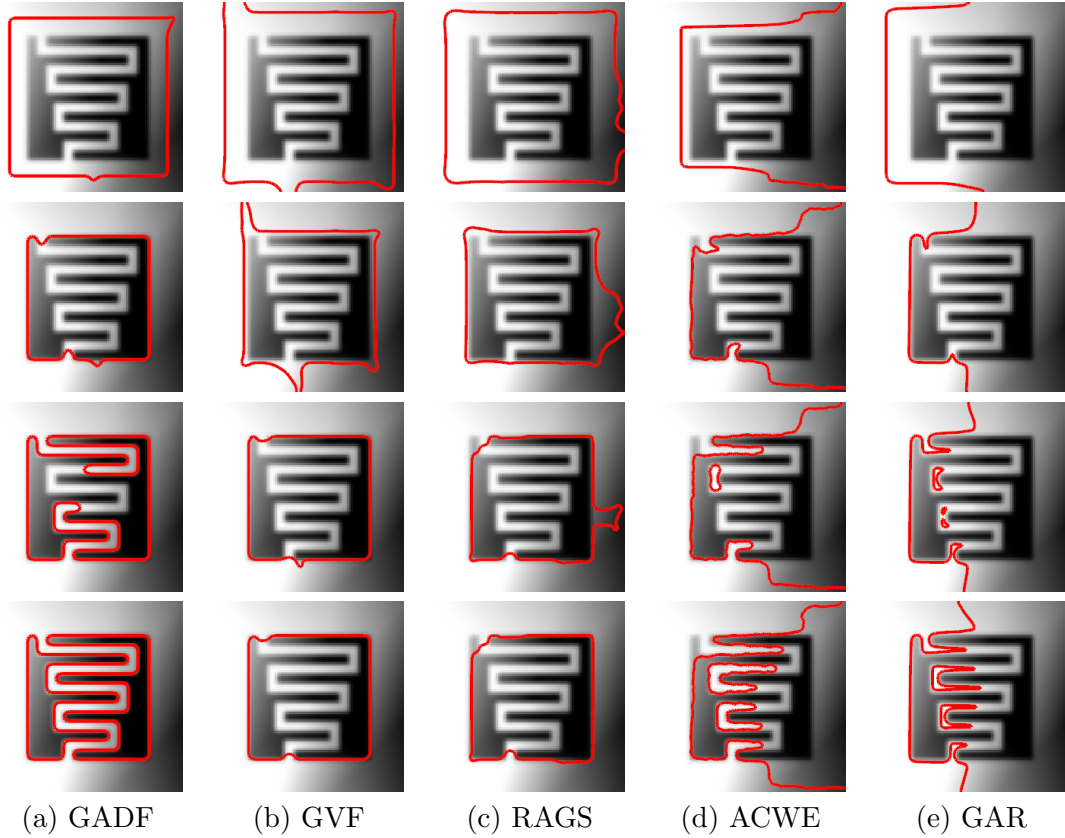


Figure 4.2: The initial contour in each method is placed at the boundary of image. The moving contours are shown from top to bottom. The illumination is changed on the object and its background. The GADF clearly captures the object. Note that the region map in the RAGS is almost same as the object. The ACWE in (d) may capture the object by manipulating four parameters in the formulation (2.6), however, it does not work with  $\lambda_1 = \lambda_2 = 1$ ,  $\alpha = 0.01$ , and  $\eta = 0$ . The simplified version of the GAR [30] in (e) does not capture the rectangle because the Gaussian distribution is not adjustable to represent the varying illumination.

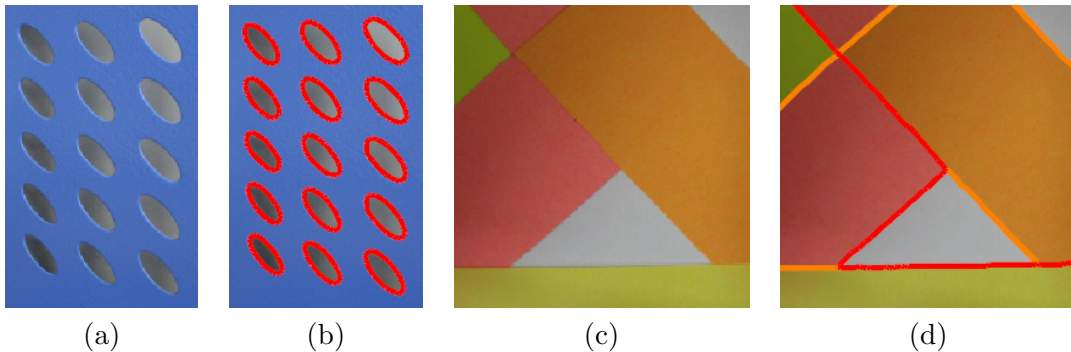


Figure 4.3: Multiple junctions and holes are captured by the proposed model. Note that the varying illumination on each hole is caused by the shadow. It makes the same difficulty to capture the object as in Figure 4.2.

direction. It prevents the leakage on the weak edges and it captures highly concave boundaries of objects. As the problem of GVF is shown by Gil and Radeva [10], the contour from the GVF does not move into the concave part of the object. Even though the region map in the RAGS is almost same as the objects, it does not capture the object because of the same reason in the GVF. Since the illumination is changed, it is not easy to find the proper combination of parameters in the ACWE in order to capture the object. The simplified version of GAR [30] does not capture the object because the Gaussian distribution is not adjustable to represent the varying illumination.

Figure 4.3 shows examples of multiple junctions and holes. Since the proposed model uses initial dual level set functions and two different binary balloon forces, it captures holes and multiple junctions. The varying illumination on each hole in Figure 4.3-(a) is caused by the shadow. It makes the same difficulty to capture the object as in Figure 4.2. The multiple junctions are easily captured by the extension of ACWE and GAR to multiple level set framework with the mutually exclusive force [13, 16].

Table 4.1 shows the robustness for different noise levels. We use the star shape  $r = 35 + 8 \cos(5\theta)$  in the polar coordinate. The center of the star shape is placed at the center of the 100 by 100 image. The Gaussian white noise is added with the zero mean and the different values of the standard deviation  $\sigma$  from 10 to 100. The accuracy is computed by using the relative length:

$$\text{Rel. length} \equiv \frac{1}{|\Omega^e|} \int_{\Omega^e} |\phi^n(x) - \phi_e(x)| dx, \quad (4.2)$$

where  $\Omega^e = \{x \in \Omega \mid |\phi_e(x)| \leq 1.5\}$ ,  $\phi_e$  is the numerical solution of the proposed model without noise, and  $\phi^n$  is the solution with  $\sigma \geq 10$ . The accuracy in the proposed model is due to the nonlinear structure tensor from Brox *et al.* [32]. GAR and ACWE are strongly robust to noise and GVF, GAC, and RAGS can also capture the object in the noisy image if the proper Gaussian smoothing operator is used to denoise the image in the preprocessing.

In Figure 4.4, we show real photos which are taken in the photo studio. They have several difficulties in the segmentation. The object has multiple junctions and holes. Due to the lighting condition, the illumination is changed in all images. Moreover, the shadow


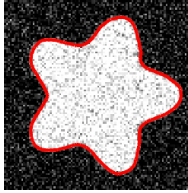


$\sigma$	Rel. length		
10	3.162852e-2		
20	9.240673e-2		
30	1.346118e-1		
40	1.378111e-1		
50	2.005598e-1		
60	2.290991e-1		
70	3.096217e-1		
80	3.848278e-1		
90	3.481178e-1		
100	3.842960e-1		

Table 4.1: It shows the robustness of the proposed algorithm to different noise levels. The Gaussian white noise is added with the zero mean and the different values of the standard deviation  $\sigma$  from 10 to 100. The accuracy is computed by using the relative length in (4.2). The images on the right show different noise levels, from the top left to the bottom right,  $\sigma = 20$ ,  $\sigma = 50$ ,  $\sigma = 70$ , and  $\sigma = 100$ .

and the reflection on objects make weak edges along the boundary of objects. The contour in the result captures the major part of the boundary. In Figure 4.5 the proposed model is used to capture the object in natural images [1,2] which have more severe difficulties in the segmentation. The images in Figure 4.5 have simple colors on background or objects. Even though the proposed model successfully detects most of boundaries in the main object, it cannot capture a very thin object which has a thickness of only few pixels in the image. Since the thin object like a line segment is not enclosed by the edge points (3.1), the binary balloon force does not have different values across the object. It causes that the evolving contour passes by its boundary which is almost the same as the object itself; see the first row in Figure 4.5. We note that it is necessary to study the proper final time in the nonlinear diffusion process (3.4). If the final time is long enough, the smoothing effect on vague boundaries deteriorates the orientation of GADF and the evolving contour passes by such boundaries; see the third row in Figure 4.5. The reason we cannot use a short final time is that most of images have noise which makes inaccuracy for computing the GADF even though it is small amount.

## 5 Conclusions

The proposed model is based on the main framework of active contours which have been mostly used in image segmentation. After we found common terms which play the same role in the view of forces to evolve contours, we proposed the GADF, the binary edge function, and the binary balloon force. They are combined into the proposed model in order to detect boundaries of objects in many difficult cases, such as varying illumination and complex shapes. The GADF is the vector flow obtained by a geometric analysis of eigenspace in a diffused tensor field on a color image as a two-dimensional manifold. The exact locations of



Figure 4.4: The images are taken in the photo studio. The objects are commercial products, the first row is a part of DVD player and the others are parts of a component in a machine. Even though the objects are taken on the simple background, there are well-known difficulties in image segmentation: the weak edge and complexity of shapes such as holes and multiple junctions. Note that weak edges are shown in the right side of DVD in the first row and the bottom of the object in the last row. The proposed model clearly captures boundaries of objects.

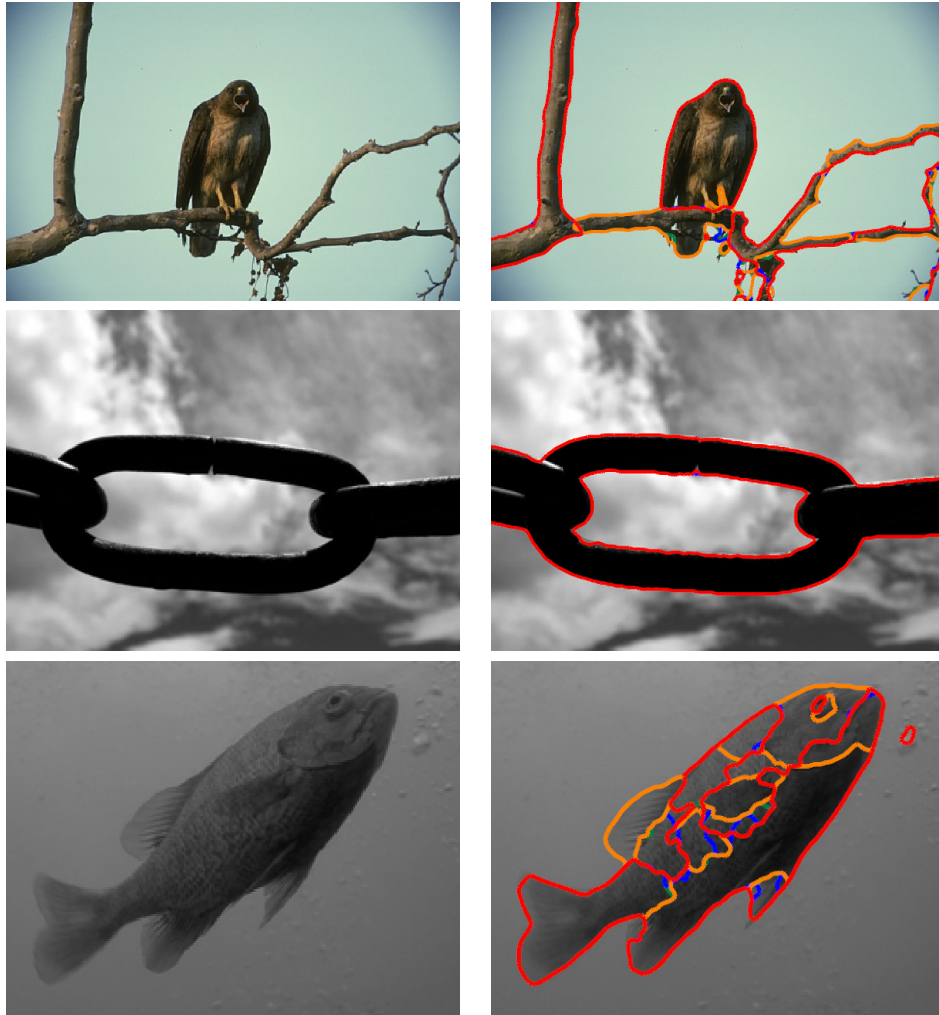


Figure 4.5: We use some of images from [1, 2]. The proposed model captures the object in each image. The holes in the object and multiple junctions from different colors are detected, but some of thin branch in the first row and the left ventral fin of the bream in the third row are not clearly segmented.

boundaries are defined by the GADF. The orientation of GADF is orthogonally aligned with the boundary of object and two vectors across the boundary have the opposite direction. It prevents the leakage on the weak edge even though the illumination is changed. To reduce the interference from other forces, we designed the binary edge function obtained by the property of orientation in the GADF. We also designed the binary balloon force based on the four-color theorem. They have just two values, 1 or  $-1$ , which mean that contours are expanded or shrunk. The main goal of the binary balloon force is to move the initial contours toward boundaries of object regardless of positions of the contours. Combining with initial dual level set functions, it is possible that contours from the proposed model capture holes in objects and multiple junctions from different colors of objects. The result does not depend on positions of initial contours.

## Acknowledgments

The authors would like to thank technical staffs of INTVIM for providing images taken in their studio.

## References

- [1] S. Alpert, M. Galun, R. Basri, and A. Brandt. Image segmentation by probabilistic bottom-up aggregation and cue integration. In *CVPR07*, pages 1–8, 2007.
- [2] D. Martin, C. Fowlkes, D. Tal, and J. Malik. A database of human segmented natural images and its application to evaluating segmentation algorithms and measuring ecological statistics. In *Proc. 8th Int'l Conf. Computer Vision*, volume 2, pages 416–423, July 2001.
- [3] M. Kass, A. Witkin, and D. Terzopoulos. Snakes: Active contour models. *Int. J. Comput. Vis.*, 1:321–331, 1988.
- [4] V. Caselles, F. Catté, T. Coll, and F. Dibos. A geometric model for active contours in image processing. *Numer. Math.*, 66:1–31, 1993.
- [5] V. Caselles, R. Kimmel, and G. Sapiro. Geodesic active contours. *Int. J. Comput. Vis.*, 22:61–79, 1997.
- [6] S. J. Osher and J. A. Sethian. Fronts propagating with curvature dependent speed: Algorithms based on Hamilton-Jacobi formulations. *J. Comput. Phys*, 79:12–49, 1988.
- [7] C. Xu and J. L. Prince. Snakes, shapes, and gradient vector flow. *IEEE Trans. Image Processing*, 70:359–369, 1998.
- [8] C. Xu and J. L. Prince. Generalized gradient vector flow external forces for active contours. *Signal Processing*, 71:131–139, 1998.
- [9] C. Xu, A. Yezzi, and J. L. Prince. On the relationship between parametric and geometric active contours. In *Proc. of 34<sup>th</sup> Asilomar Conference on Signals, Systems, and Computers*, pages 483–489, 2000.

- [10] D. Gil and P. Radeva. Curvature vector flow to assure convergent deformable models for shape modelling. In *Lecture Notes in Computer Science, Springer Verlag, Proceedings of EMMCVPR, Lisbon, Portugal 2003*, 2003.
- [11] Z. Yu and C. Bajaj. Normalized gradient vector diffusion and image segmentation. In *Lecture Notes In Computer Science 2352*, pages 517–530, 2002.
- [12] X. Xie and M. Mirmehdi. RAGS: Region-aided geometric snake. *IEEE Trans. Image Processing*, 13:640–652, 2004.
- [13] L. Vese and T. Chan. A multiphase level set framework for image segmentation using the Mumford and Shah model. *Int. J. Comput. Vis.*, 50:271–293, 2002.
- [14] T. Chan and L. Vese. Active contours without edges. *IEEE Trans. Image Processing*, 10:266–277, 2001.
- [15] N. Paragios and R. Deriche. Geodesic active regions and level set methods for supervised texture segmentation. *Int. J. Comput. Vis.*, 46:223–247, 2002.
- [16] N. Paragios and R. Deriche. Geodesic active regions: A new framework to deal with frame partition problems in computer vision. *J. Vis. Commun. and Image Represent.*, 13:249–268, 2002.
- [17] L. D. Cohen. On active contour models and balloons. *CVGIP: Image Understanding*, 53:211–218, 1991.
- [18] R. Adams and L. Bischof. Seeded region growing. *IEEE Trans. Pattern Anal. Machine Intell.*, 16:641–647, 1994.
- [19] S. C. Zhu and A. Yuille. Region competition: unifying snakes, regions growing, and Bayes/MDL for mutiband image segmentation. *IEEE Trans. Pattern Anal. Machine Intell.*, 18:884–900, 1996.
- [20] N. Robertson, D. P. Sanders, P. Seymour, and R. Thomas. The four color theorem. *J. Combin. Theory, Ser. B*, 70:2–44, 1997.
- [21] K. Appel and W. Haken. Every planar map is four colorable. Part I. Discharging. *Illinois J. Math.*, 21:429–490, 1977.
- [22] A. J. Abrantes and J. S. Marques. A class of constrained clustering algorithms for object boundary extraction. *IEEE Trans. Image Processing*, 5:1507–1521, 1996.
- [23] N. Paragios, O. Mellina-Gottardo, and V. Ramesh. Gradient vector flow fast geometric active contours. *IEEE Trans. Pattern Anal. Machine Intell.*, 26:402–407, 2004.
- [24] M. G. Crandall, H. Ishii, and P. L. Lions. User’s guide to viscosity solutions of second order partial linear differential equations. *Bulletin of the American Math. Society*, 27:1–67, 1992.
- [25] D. Mumford and J. Shah. Optimal approximation by piecewise smooth functions and associated variational problems. *Commun. Pure Appl. Math.*, 42:557–685, 1989.



- [26] A. Yezzi, A. Tsai, and A. Willsky. A fully global approach to image segmentation via coupled curve evolution equations. *J. Vis. Commun. and Image Represent.*, 13:195–216, 2002.
- [27] J. Lie, M. Lysaker, and X.-C. Tai. A variant of the level set method and applications to image segmentation. *Mathematics of computation*, 75:1155–1174, 2006.
- [28] S.-H. Lee and J. K. Seo. Level set-based bimodal segmentation with stationary global minimum. *IEEE Trans. Image Processing*, 15:2843–2852, 2006.
- [29] A. Chakraborty, H. Staib, and J. Duncan. Deformable boundary finding in medical images by integrating gradient and region information. *IEEE Trans. Medical Imaging*, 15:859–870, 1996.
- [30] M. Rousson and R. Deriche. A variational frame work for active and adaptive segmentation of vector valued images. Technical report, Research Report, N. 4515, INRIA, July 2002.
- [31] H. Zhao, T. Chan, B. Merriman, and S. Osher. A variational level set approach to multiphase motion. *J. Comput. Phys.*, 127:179–195, 1996.
- [32] T. Brox, J. Weickert, B. Burgeth, and P. Mrázek. Nonlinear structure tensors. *Image and Vision Computing*, 24:41–55, 2006.
- [33] M. Rousson, T. Brox, and R. Deriche. Active unsupervised texture segmentation on a diffusion based feature space. In *Proc. 2003 IEEE Computer Society Conf. on Computer Vision and Pattern Recognition*, volume 2, pages 699–704, 2003.
- [34] D. Peng, B. Merriman, S. Osher, H. Zhao, and M. Kang. A PDE-based fast local level set method. *J. Comput. Phys.*, 155:410–438, 1999.
- [35] J. Weickert, B. M. ter Harr Romeny, and M. A. Viergever. Efficient and reliable schemes for nonlinear diffusion filtering. *IEEE Trans. Image Processing*, 7:398–410, 2001.
- [36] G. Aubert and P. Kornprobst. *Upwind differencing schemes for hyperbolic conservation laws with source terms*. Springer-Verlag, New York, 2002.
- [37] D. Comaniciu and P. Meer. Mean shift: A robust approach toward feature space analysis. *IEEE Trans. Pattern Anal. Machine Intell.*, 24:603–619, 2002.